CRACK GROWTH ANALYSIS OF FIBER METAL LAMINATES STIFFENED PANELS

Pedro Humberto Wüst Félix[1], Mariano Andrés Arbelo[1] and Marcelo Ricardo Bertoni Rodrigues[2]

[1] Instituto Tecnológico de Aeronáutica
[2] EMBRAER - Empresa Brasileira de Aeronáutica

Abstract: The use of fiber metal laminates stiffened panels for aerospace application has been largely increasing due to its low crack propagation rate and excellent residual strength behavior. In order to compare the traditional built up aluminum constructed stiffened panels and fiber metal laminates materials under the context of damage tolerance, two stiffened panels are design, tested and compared against finite element models: (1) aluminum skin with riveted stringers and (2) fiber metal laminate skin with bonded stringers. The two panels exhibited significantly different results, with the fiber metal laminate stiffened panel having the best response in both crack propagation and residual stress. With the objective of obtaining an accurate analysis tools for these two panels, filling a gap of available commercial softwares, detailed Finite Element Models are built aiming the use of Virtual Crack Closure Technique to obtain Stress Intensity Factors, taking into account the delamination phenomenon during crack propagation on fiber metal laminates materials. Numerical results show that the proposed technique is able to reach good correlation and it is observed that the chosen delamination shape largely dictates crack growth behavior on the fiber metal laminates stiffened panel.
Keywords: Stiffened Panels; FML Delamination; VCCT; Glare; Crack Growth

INTRODUCTION

Aircraft structures must be light, strong, and durable: that's the structural engineer paradigm. Conceiving and building such structures allows higher payloads to be lifted. For achieving this feature, lightweight construction concepts are applied, transferring the proper loads to each component of the structure. To build main structural parts such as wings and fuselages, components as stringers, skin, and frames must be fastened or built together, characterizing both built-up and integral structures [1].

The architecture of these built up structures is still mainly composed of reinforced panels, with better shape optimization achieved from improvements in manufacturing techniques and analysis capabilities, along with different materials and attachment techniques such as bonded stringers. However, the fatigue and crack propagation problem perceived since the first airliners is still present. A good Damage Tolerance analysis of panels is capable of mitigating this problem, building safe and light skin-stringer structures [2,3,4].

One important parameter on crack growth and Damage Tolerance design is the crack growth rate of the material. Crack growth rates determine the frequency of inspections through crack growth and residual

Pedro Félix al. This is an open-access article distributed under the terms of the Creative Commons Attribution 3.0 United States License, which permits unrestricted use, distribution, and reproduction in any medium, provided the original author and source (in this case: Proceedings of the 31st symposium of ICAF - the International Committee on Aeronautical Fatigue and Structural Integrity, Delft, 26-29 June 2023) are credited.

strength analysis. Materials with higher rates demand smaller inspection intervals in order to increase safety, therefore raising costs to airliners [2,3].

Fiber Metal Laminates (FMLs) have a good fatigue response due to different crack growth mechanisms as found in monolithic metals, presenting a linear crack growth rate in contrast to common exponential crack growth rates found in monolithic metals. FMLs are composites built by laminating aluminum interchanged with polymeric fiber layers. The most prominent FML layup is Glare® (Glass Reinforced Aluminum). This composite shows great flammability and impact resistance, along with good cohesion between its layers, which fits for fuselage requirements for the A380's upper fuselage. The fiber stacking sequence constitutes the Glare®'s grade, and greatly changes material response to fatigue, stiffness, and residual strength [6].

FML characteristics improved life is reached through the load bridging behavior, once during cyclic load appliance the fiber layers remain intact, while cracks are propagated on aluminum layers only. The loads are then transferred from the aluminum layers to the glass fiber layers, mainly on the crack tip region, slowing crack growth [6]. This effect is illustrated in Figure 1.

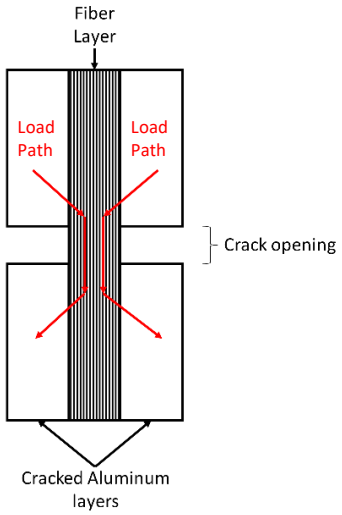

Figure 1 Load bridging occurred in FMLs

The bridging behavior is achieved through delamination of the layers, which accompanies crack growth, visually as a wake, with its root proportional to the size of the crack. The delamination occurs due to large interlaminar stresses at the adhesive interface, enough to break the bonding [6].

Since Glare® sheets are meant to be used as skin elements in built-up construction, they can be stiffened as monolithic aluminum sheets to improve both damage tolerant and stability properties. Stiffeners arrest effect on cracks is illustrated in Figure 2, and act as an alternative load path when the skin is damaged, thus improving the residual strength of the panel [1,4].

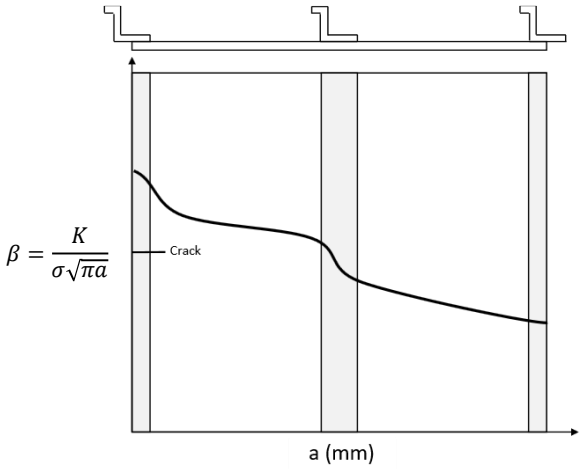

Figure 2 Stringer effect factor β used in the Stress Intensity Factor equation, where β=K/(σ√πa) is the geometric correction factor [5].

For monolithic metals, there are many closed form solutions for Stress Intensity Factors in simple geometries, and techniques such as superposition and composition may be used to obtain these values, if a better description of geometric and boundary conditions is needed. Another way out of this problem is through construction of Finite Element (FE) models, which can take in account several geometric factors and nuances during crack growth simulation using energy release techniques [5].

FMLs however, do not possess such simple and straightforward methods, once many other variables affect the Stress Intensity Factors at the crack tip, such as number of layers, fiber direction and type, and aluminum over polymer thickness. Analytical methods have been proposed to predict crack growth along fiber delamination, starting from studies performed on ARALL in the 80's, being followed by Glare® in the early 2000's. These methods account for the displacement compatibility of the constituent materials around the crack, for each crack size. The crack growth process follows a Paris law for the metal sheets and an energy release formulation is used to determine the compatible delamination to the obtained crack size. This process is iterative and numerically solved, obtaining the bridging stresses distribution on the fiber layers [6].

As a follow-up of this method, an energy release method similar to the one used for crack growth analysis in monolithic panels can be proposed. This model would however take delamination into account, incorporating both phenomena (crack and delamination) simultaneously.

In this context, this works aims to: a) Compare FML reinforced panels crack growth behavior when compared to monolithic aluminum reinforced panels through experimental testing, obtaining crack growth rates and number of cycles to failure, and b) Propose a crack growth analysis procedure for FML purely through Finite Elements modelling.

SPECIMENS, EXPERIMENTAL SETUP AND CRACK PROPAGATION TESTS

To verify the numerical approach to be introduced in this work, a detailed experimental analysis was carried-out to provide reliable experimental data for comparison. Two stiffened panels are built and tested to further investigate crack growth behavior: (1) monolithic aluminum skin with riveted stringers (codenamed REB) and (2) FML skin (Glare®) with glued stringers (codenamed FML).

Specimen's geometry has the dimensions shown in Figure 1, for both stiffened panels. Each plate has 5 stringers attached, with the central stringer being cut to simulate complete failure. The skin of the stiffened panel has a 6mm circular notch and a 12 mm cut to simulate a small initial crack. Anti-bending bars were positioned next to the crack growth region, in contact with

stringers and skin, to simulate pure Mode I loading on the crack growth zone by avoiding out of plane bending caused by the stiffened panel's inherent asymmetry.

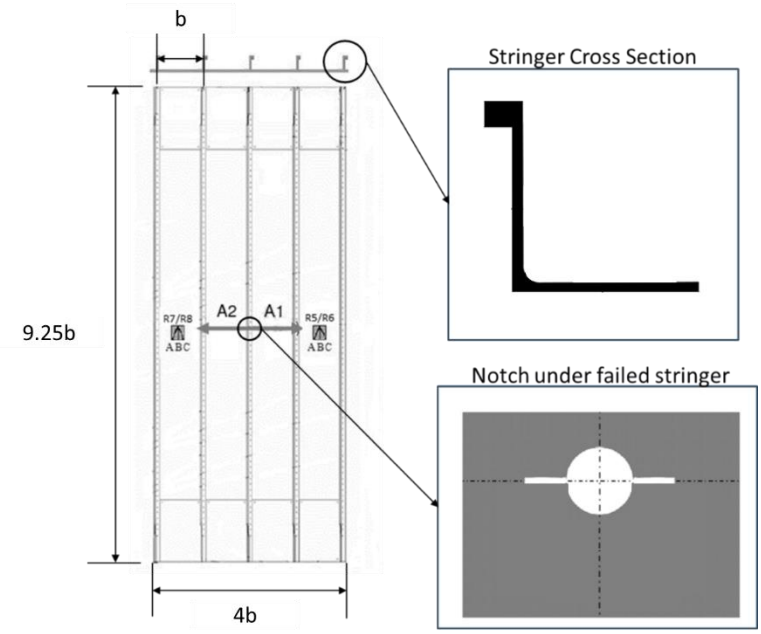

Figure 1 Plate and stringer geometry – with A1 and A2 as the two crack front directions

The materials used in each stiffened panel are shown in Table 1, along with the stringer connection methodology. The Glare® layup used in the FML plate is shown in Table 2, where 0° corresponds to the longitudinal direction of the stiffened panel.

Table 1 Stiffened panel materials

Panel	Plate Material and Thickness	Stringer Interface	Stringer material
Riveted	Al 20XX, 1.25mm	Al 21XX Rivets, 3.969 mm	Al 70XX
Glare	Glare®2A – 2/1 – 0.4, 1.06mm	Cytec Adhesive	Al 70XX

Table 2 Glare® skin layup

Ply	Material and Thickness	Orientation
1	Al 20XX, 0.4 mm	-
2	Glass Fiber tape	0°
3	Glass Fiber tape	0°
4	Al 20XX, 0.4 mm	-

The experimental tests were conducted using a servo-hydraulic testing machine with 2Hz cyclic load application frequency and R = 0.1 (minimum over maximum load ratio), applying a Pmax load to the riveted stringer panels and 1.2 Pmax to the FML panel to induce a gross stress on the aluminum sheet compatible with a common stress value found in fuselage skins under

service and an initial stress intensity factor of 500 $MPa\sqrt{mm}$ on the riveted panels, and 600 $MPa\sqrt{mm}$ on the FML panel.

Applied load, displacement, crack length and strain distribution along the specimens were measured during the crack growth test and residual strength test by a load cell, displacement sensors, a couple of crack gages and rosettes glued in the adjacent bays from the cracks site, for far field strain reading. Crack size was visually monitored as well using a couple of CCD cameras, one for each crack front. The crack propagation results are shown in Figure 2, for each panel and crack front.

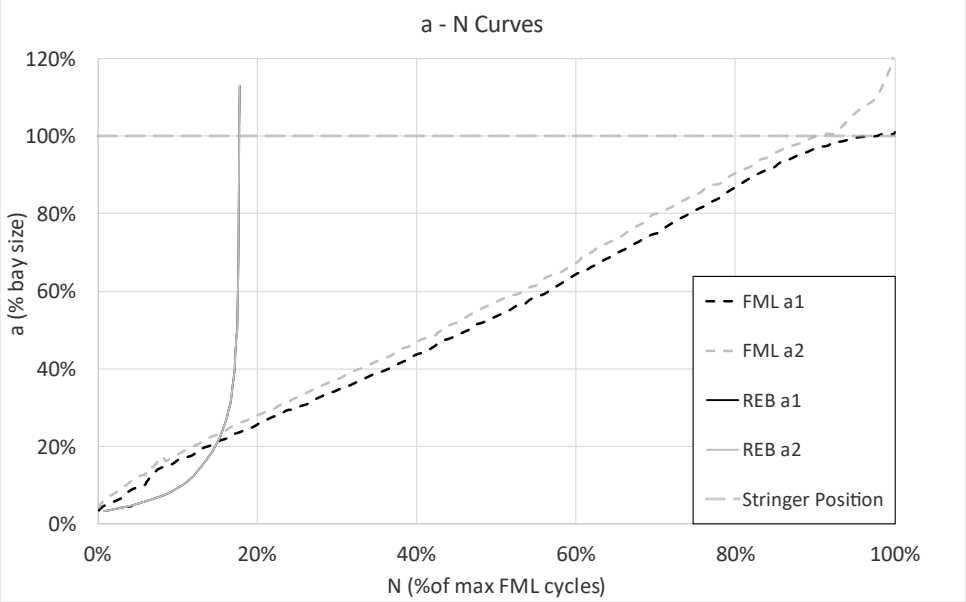

Figure 2 Crack propagation result for each stiffened panel and crack front

As expected, the stiffened panel with FML skin required a much larger number of cycles to obtain the same crack size than the stiffened panel with monolithic aluminum skin and riveted stringers (REB). It is also interesting to notice that a constant crack growth rate (da/dN) value of $8x10^{-4}mm/cycle$ is observed in the FML stiffened panel and happens until near the stringers region, where load is redistributed. Such linear behavior is observed in literature due to the mentioned bridging mechanism [6].

The FML panels crack size up to 25 mm was read through crack gages, thus generating the data offset at the beginning the displayed crack propagation curve. From this crack size onward, data was obtained through Digital Image Correlation (DIC).

A constant value of da/dN implies in a constant Stress Intensity Factor. This value can be obtained by solving any da/dN equation backwardly, such as Forman's. The value obtained for this experiment is calculated in Section 0.

A residual strength test followed each crack propagation test. The experimental setups are shown in Figure 3.

Figure 3 Experimental test setup for fatigue (left) and residual strength (right) characterization

The experimental results from the residual strength tests are shown on Figure 4, were the applied load, and crack growth are measured until final fracture.

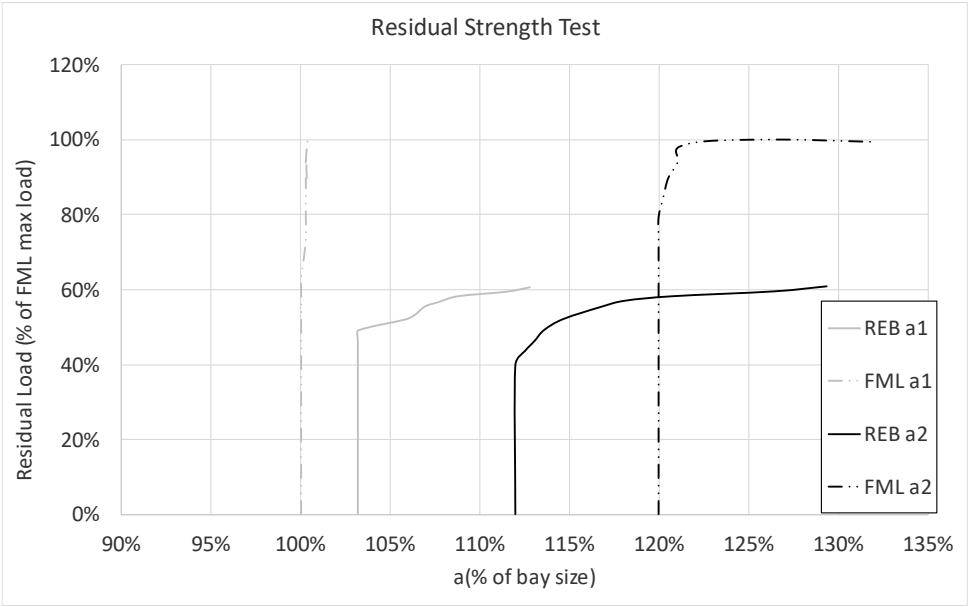

Figure 4 Residual strength test results.

NUMERICAL APPROACH – FINITE ELEMENT MODELS

The softwares of choice for this work were MSC Nastran 2016 solver and FEMAP v.12 modelling interface, the last due to its customization capabilities. The basic nonlinear solution (SOL 106) was used with large displacements enabled due to the large geometrical nonlinearities observed in the test. Linear elastic material properties were adopted through all numerical simulations.

Finite element models for both stiffened panels were built using a common baseline model, with identical geometry to the tested panels. In general, the skins were built using linear plate elements (CQUAD4), 3mm size on refinement region (where crack propagation occurs) and 9 mm on coarse region (outside the crack propagation region). This element size was chosen after

a convergence analysis and due to constructive constraints, such as coincident node positions between skin and stringers at the rivet positions.

Only half of each stiffened panel was model, using the crack propagation plane as symmetry plane (XZ plane), with constraints on Y translation, X and Z rotations. The loads were applied through a rigid element (RBE2) in Y direction only and constraining the independent node's displacement and rotations in directions Tx, Tz, Rx and Ry, imposing the same constraints as observed in tests. To simulate the anti-bending setup applied during experimental tests, linear gap elements were created on the same regions as the bars were positioned in tests, thus avoiding out of plane movement. A schematic of the model is shown in Figure 5.

The stringer had its flanges and webs modeled in plate elements, while the bulb was modeled in bar elements (CBAR), ignoring its offset. Plate offsets were applied to separate the stringers from the skin elements.

To apply the Virtual Crack Closure Method, a node release region was determined, where nodes were gradually and sequentially released from its constraints, simulating an incremental crack growth. The simulated crack ran symmetrically on both sides.

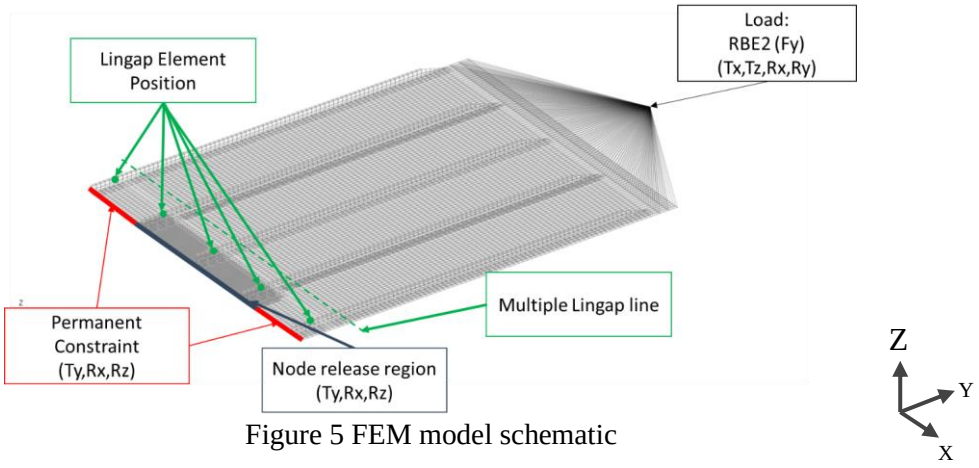

Figure 5 FEM model schematic

The connection between plates and stringers was made through different approaches: the riveted panel was connected by nodes on rivet positions, through spring elements (CBUSH) with constants calculated by Douglas' formulation (SWIFT, 1971) exhibited in Equations 1,2 and 3:

$$F = \frac{A}{E_f d} + B\left(\frac{1}{E_1 t_1} + \frac{1}{E_2 t_2}\right) \quad (1)$$

$$k_{trans} = \frac{1}{F} \quad (2)$$

$$k_{axial} = \frac{E_f A_{cs}}{t_1 + t_2} \quad (3)$$

with dimensionless factors A = 5 and B = 0.8 material constants for aluminum, d the rivet diameter (mm), E_f the fastener modulus of elasticity (MPa), E_1 and E_2 the elastic modulus of the connected plates (MPa), t_1 and t_2 the plates thicknesses (mm) and A_{cs} the cross section area of the rivet, resulting on the stiffness shown in Table 3. Bending stiffness was simply doubled from shear since there was no formulation for it in reference presented above. The Glare®

sheets were connected to the stringers via coincident nodes, simulating a rigid connection and neglecting the shear deformation of the adhesive layer. Connections are shown in Figure 6.

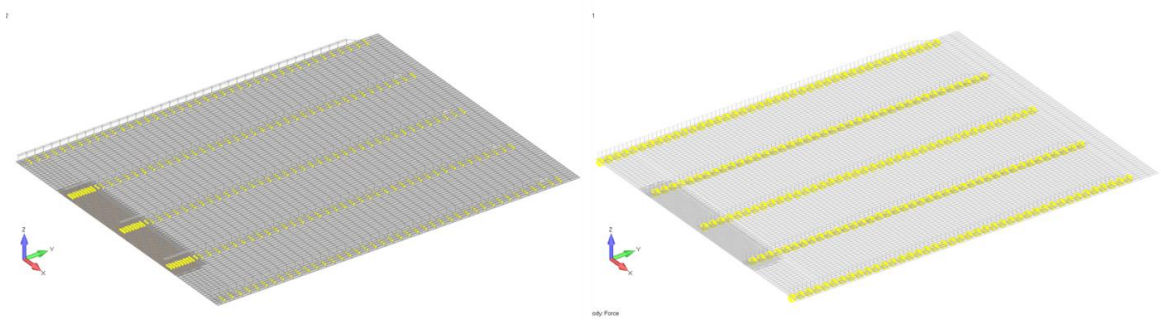

Figure 6 Connection regions on riveted panel - REB (left, single element) through spring element and bonded panel - FML (right) through coincident nodes.

Table 3 Calculated stiffness for riveted panel model.

Panel	$k\left(\frac{N}{mm}\right)$
Shear	28
Axial	343
Bend	686

The Glare® skin of the FML stiffened panel model was made using 3 layers of coincident plate elements, each discriminated by an offset value simulating a composite layup. A delamination region was determined according to the maximum delamination length observed in test. Outside this region, all nodes were merged for faster processing, while in delamination region all nodes were connected via MPC, with nodes from each layer being identified through a numbering range, as shown in Figure 7.

To simulate the delamination phenomenon, a straightforward method was proposed where a linear correlation between the crack size and the delamination area is used, considering a predetermined proportion, assuming a delamination shape through crack length. The crack was grown in both aluminum layers symmetrically on both flanks and following the node releases occurring on the crack front, the MPC interface between layers was also undone as the cracks propagates, simulating the adhesive failure, illustrated in Figure 8. Four delamination shapes were studied as they are also used in the available analytical method: triangular, elliptical, cosinoidal and parabolic, as shown in [6].

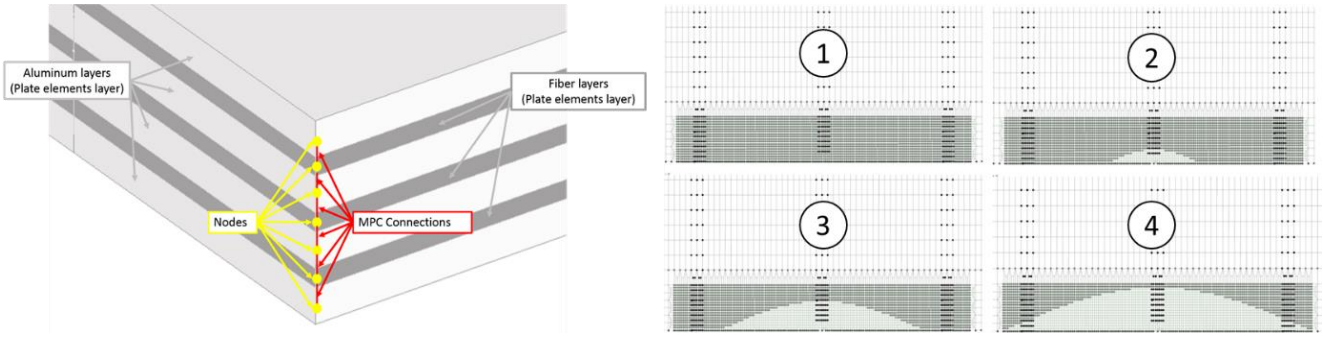

Figure 7 MPC connection by layer on Glare® model (left) and forced delamination sequence, cosine shape (right)

Material data for the models was gathered from MMPDS [9], including the stress-strain curve of Al 7050-T76511.

ANALYSIS METHODOLOGY

Virtual Crack Closure Technique (VCCT) was used to obtain the release energy in crack front only. In this method, using the same Finite Element model, two analyses are done for a given crack size: (i) one to obtain required reaction forces on the nodes at the crack tip, (ii) another to obtain the displacement field of the same nodes after the displacement constrain is release under the same load, as shown in Figure 8. The work needed to open the crack is calculated as shown in Equation 4. The relation between the work (ΔU) and the energy release rate (G) follows Equation 5 [7]:

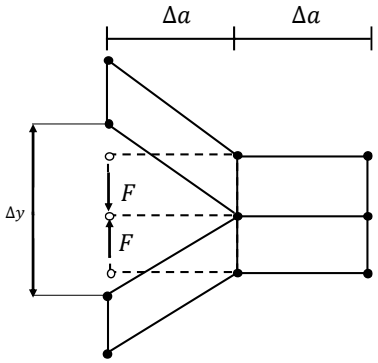

Figure 8 VCCT analysis in FEM mesh, collecting forces before mesh opening and displacements after mesh disconnection [5].

$$\Delta U = \frac{1}{2}(F.\Delta y) \qquad (4)$$

$$G = \frac{\Delta U}{\Delta a.t} \qquad (5)$$

With Δa been the crack growth increment and t the plate thickness. Finally, for a pure Mode I crack growth and plane stress, the relation between G and the Stress Intensity Factor (SIF) K is given by Equation 6 [8]:

$$G = \frac{K^2}{E} \qquad (6)$$

Where E is the material elastic modulus. Obtaining both the maximum and minimum values of SIF through linear scaling of the maximum and minimum loads applied, the crack growth derivative da/dN can be calculated through the Forman equation, and further integration of these values can be used to calculate the crack size vs number of cycles ($a\ x\ N$) curve [8].

$$\frac{da}{dN} = \frac{C_2 \Delta K^m}{(1-R)K_c - \Delta K} \quad (7)$$

Where the stress intensity factor ΔK is given by:

$$\Delta K = \beta \Delta \sigma \sqrt{\pi a} \quad (8)$$

With the R the proportion between maximum and minimum stresses applied. The constants used on Forman equation are obtained from the open literature: $K_c = 3478.51\, MPa\sqrt{mm}$, $m = 3.38$ and $C_2 = 6.21x10^{-10}\, \frac{MPa\sqrt{mm}}{(MPa\sqrt{mm})^{m-1}}$ [8].

VCCT was also applied on the Glare® panels to obtain the Stress Intensity Factors on the aluminum layers only through calculating the reaction forces and displacements on one of the aluminum layers nodes. Different delamination shapes were tested in this work and the results were compared against the experimental delamination pattern, measured using NDT testing, as shown in Figure 9. Through this image, a b/a (delamination length at the notch root divided by crack size) relation of 0.28 was visually determined trying to compensate the irregularities on the test shape (which happened due to stringer induced torsion), being used in later analysis.

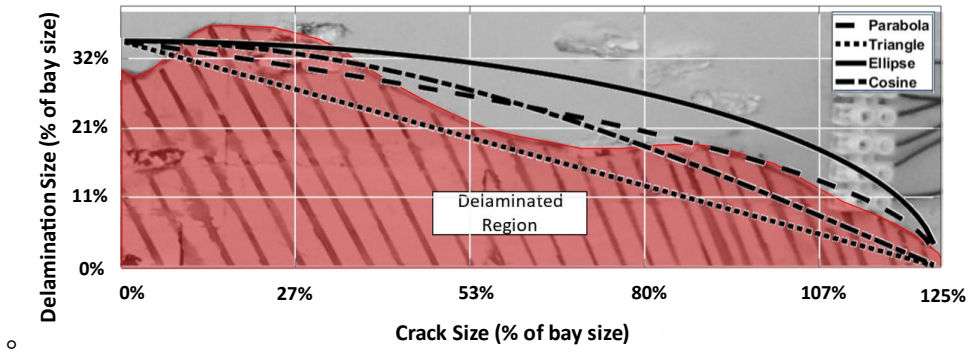

Figure 9 Numerical delamination shapes tested and compared against the experimental delamination shape, measured using NDT testing.

ANALYSIS OF RESULTS

The Stress Intensity Factor values from tests were obtained by reversing equation (7) for ΔK, with da/dN calculated from the original crack growth (axN) curve plotted from DIC measurements. This collected data is plotted in contrast to the calculated numerical results in Figure 10. Glare®'s nearly constant ΔK was plotted as a "target value" of 648.52 $MPa\sqrt{mm}$ in its respective graphs. The numerical and experimental results obtained for the riveted panel are shown in Figure 10.

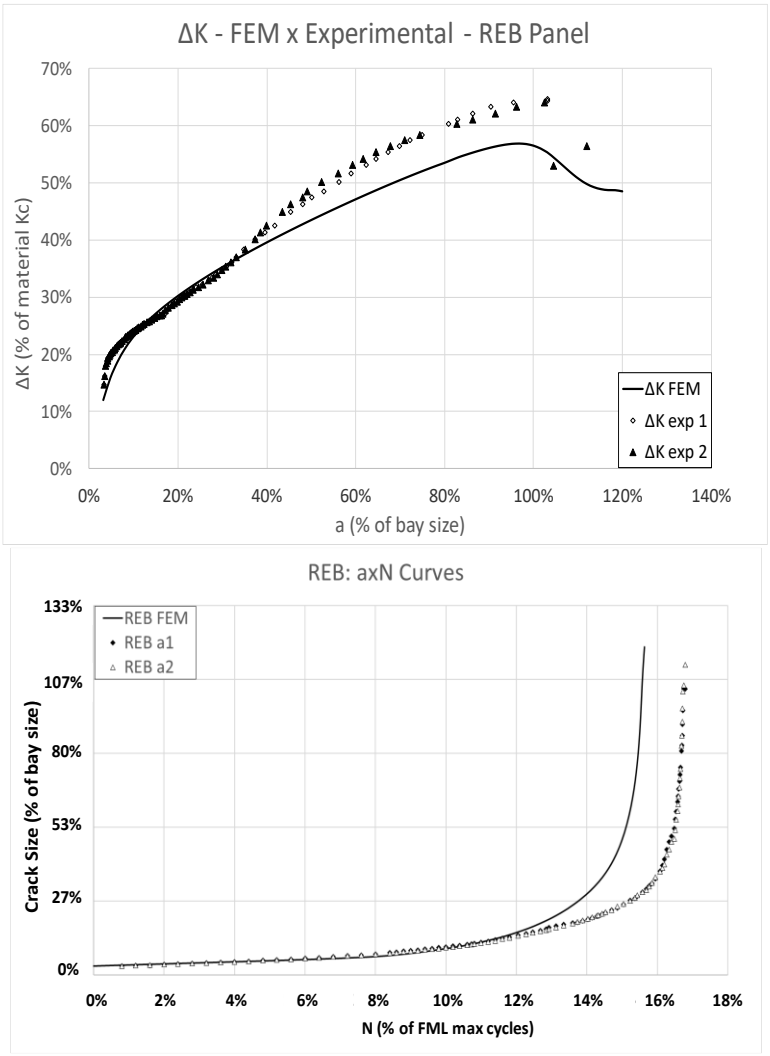

Figure 10 Analysis versus test results - Riveted Panel

A good correlation in SIF is obtained through the analysis, mainly until the crack arrest region in the stringers' vicinity. At this region, error reached a value of approximately 10%. Crack propagation results have shown very good correlation with test obtained, with an approximated error of 5% in total cycles.

The Glare® panels were then analyzed, using the different delamination shapes for crack propagation. Two analyses were performed: the first to obtain delamination shape effects in SIF behavior (Figure 11), and the second to assess the b/a proportion (delamination length on notch versus crack length) for each delamination shape (Figure 12).

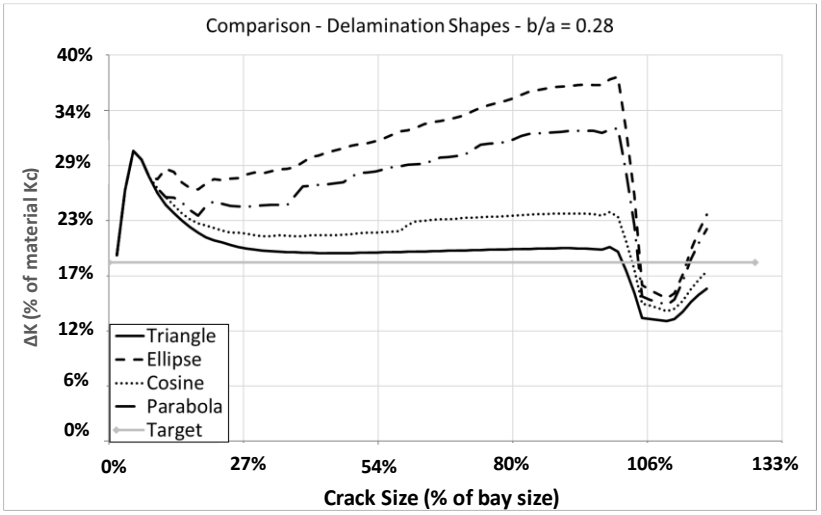

Figure 11 Stress Intensity Factor range by delamination shape

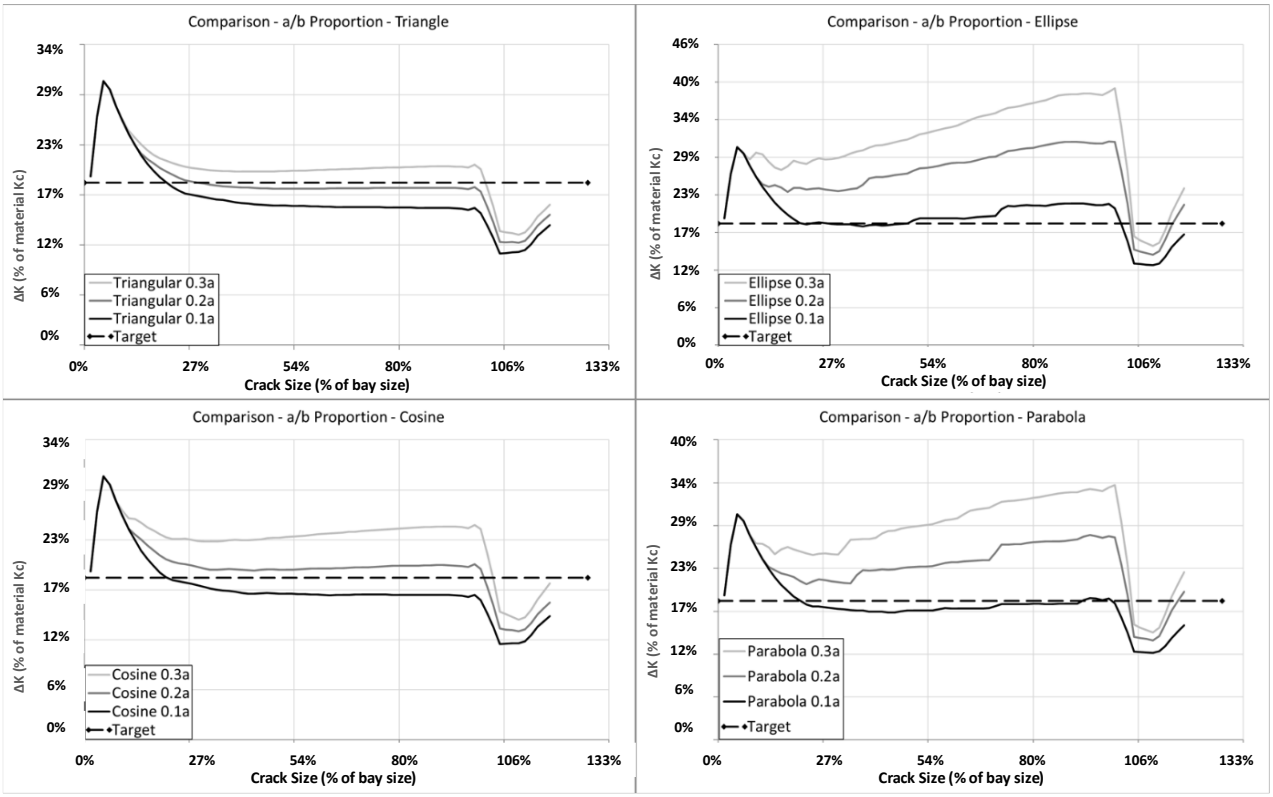

Figure 12 Sensitivity analysis - b/a proportion for each delamination shape

The performed analysis shows that the numerical model is sensitive to delamination shape, while moderately sensitive to b/a proportion. Therefore, a correct modeling of delamination is paramount for a correct analysis. Results obtained both with triangular and cosine shapes have shown the best correlation to the experimental test, with about 1% and 20% error respectively.

Results obtained in this experimental test campaign and the numerical analyses corroborate the observations present in the literature, which indicates that a larger delaminated surface causes a higher SIF in the crack tip. It is visible through Figure 9 that the ellipse shape has the largest delaminated surface, thus incurring in a larger SIF, while the triangular shape shows the opposite. Also, the b/a proportion analysis shows the same results, where a larger b/a, or a larger delamination length on the notch, causes a higher SIF value.

Since the stringer is bonded on the FML plate, the drop of the SIF at the stringer's vicinity is large, but the results obtained until the model's crack reaches this region have a constant or linear behavior as observed both in literature and tests. Plotted a-N curves using the SIF values obtained are illustrated in Figure 13.

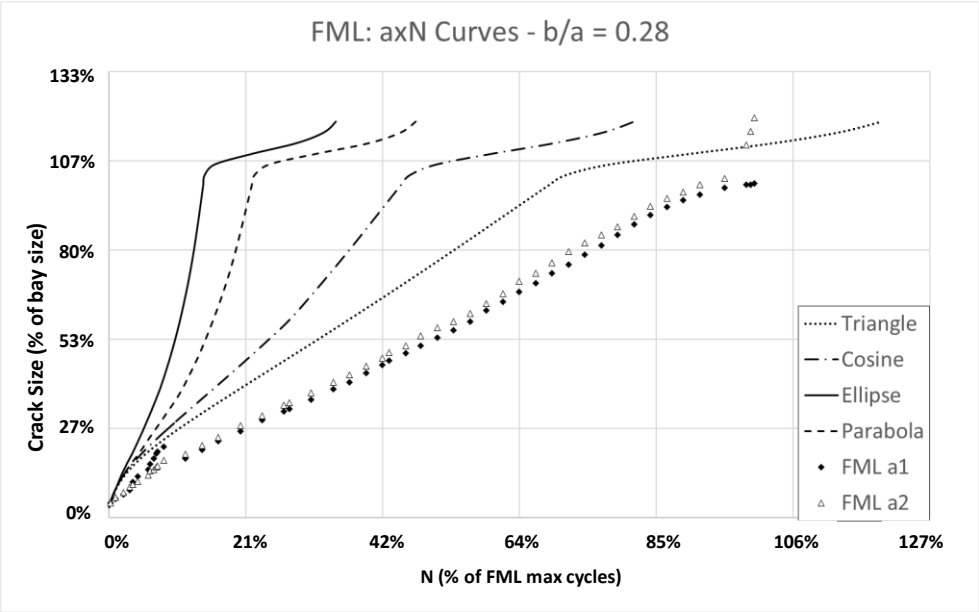

Figure 13 a-N curves obtained by delamination shape

As expected, the triangular shape shows the closest values of crack size, since its SIF behavior is closest to the one observed during the experimental test campaign. Nevertheless, the numerical results are conservative when compared to experimental tests, and most important, a constant crack propagation rate is observed in all delamination shapes.

CONCLUSIONS

In this work, a finite element methodology was developed and verified through experimental tests to calculate the fatigue crack growth of stiffened panels considering riveted and bonded joints together with FML materials for improving fatigue resistance and ultimate failure.

First, a series of dedicated finite element models were implemented at plate level to validate both: (1) VCCT approach for energy calculation and crack propagation and (2) equivalent delaminated area for laminates as a function of the crack length.

Results indicated a very good correlation of VCCT against the experimental test results. Furthermore, for stiffened Glare® plates with similar layup and loading conditions close to the ones tested on this work, delamination between aluminum and fiber glass layers seem to be well modeled with a triangular or cosine shape and a b/a proportion between 0.25-0.30, as obtained in this work's experimental study.

On a second stage of this study, the numerical models for Riveted and Glare® stiffened panels were verified against experimental results carried out in this work. Good correlation was obtained for the crack propagation, showing a conservative safety factor of 1.05 and 1.20 for triangular and elliptical shapes, respectively.

Rigid modeling of the stringers interface was proven to be conservative as presented by the great SIF drop when the crack reaches the stringer, thus demanding a better approach to the subject with elastic modeling of the interface mainly when a crack growth analysis needed next to stringer.

Finally, since the numerical models were verified for structures and stress level common to fuselage structures, the proposed methodology seams feasible for using as a fast crack propagation analysis tool for initial project and pre-sizing of fuselage structures.

ACKNOWLEDGEMENTS

Aknowledgements to Embraer and FCMF (Fundação Casimiro Montenegro Filho). This work was supported by CNPq Grant No. 311972/2020-9;
EMBRAER Research and Development team designed and manufactured the specimens, and had an important role on the definition of test proposal.

REFERENCES

[1] NIU, M. C. Airframe Structural Design. 1st. ed. Hong Kong: Conmilit Press Ltd.,1988.
[2] MOLENT, L.; DIXON B. Airframe metal fatigue revisited. International Journal of Fatigue, Volume 131, 2020.
[3] KAHLIN M., ANSELL H., MOVERARE J.; Fatigue crack growth for through and part-through cracks in additively manufactured Ti6Al4V. International Journal of Fatigue, Volume 155, 2022.
[4] RANS, C.; RODI, R.; ALDERLIESTEN, R. Analytical prediction of mode I Stress Intensity Factors for cracked panels containing bonded stiffeners. Engineering Fracture Mechanics, v. 97, p. 12-29, 2013.
[5] SCHIJVE, J. Fatigue of Structures and Materials. 2nd. ed. Delft, Netherlands: Springer, 2009.
[6] ALDERLIESTEN, R. Fatigue Crack Propagation and Delamination Growth in Glare. Phd Thesis in Aerospace Engineering - Technische Universiteit Delft, Delft, Netherlands, 2005.
[7] KRUEGER, R. Virtual crack closure technique: History, approach, and applications. Applied Mechanics Reviews, v. 57, n. 2, p. 109-143, 2004.
[8] DOWLING, N. E. Mechanical Behavior of Materials. 4th. ed. Harlow, England: Pearson, 2013.
[9] IHS. Metallic Materials Properties Development and Standardization. Columbus, USA, 2013.

RESPONSIBILITY NOTICE

The author is the only responsible for the printed material included in this paper.